

Article

Particle Number Emissions of a Euro 6d-Temp Gasoline Vehicle under Extreme Temperatures and Driving Conditions

Barouch Giechaskiel ^{1,*}, Victor Valverde ¹, Anastasios Kontses ², Anastasios Melas ¹, Giorgio Martini ¹, Andreas Balazs ³, Jon Andersson ⁴, Zisis Samaras ² and Panagiota Dilara ⁵

- ¹ European Commission, Joint Research Centre (JRC), 21027 Ispra, Italy; victor.valverde-morales@ec.europa.eu (V.V.); anastasios.melas@ec.europa.eu (A.M.); giorgio.martini@ec.europa.eu (G.M.)
- ² Laboratory of Applied Thermodynamics, Aristotle University Thessaloniki, 54124 Thessaloniki, Greece; akontses@auth.gr (A.K.); zisis@auth.gr (Z.S.)
- ³ FEV Europe GmbH, 52078 Aachen, Germany; balazs@fev.com
- ⁴ Ricardo Automotive & Industrial, Shoreham Technical Centre, Shoreham-by-Sea BN43 5FG, UK; jon.andersson@ricardo.com
- ⁵ European Commission, DG-GROW, 1040 Brussels, Belgium; panagiota.dilara@ec.europa.eu
- * Correspondence: barouch.giechaskiel@ec.europa.eu; Tel.: +39-0332-78-5312

Abstract: With the introduction of gasoline particulate filters (GPFs), the particle number (PN) emissions of gasoline direct-injection (GDI) vehicles are below the European regulatory limit of 6×10^{11} p/km under certification conditions. Nevertheless, concerns have been raised regarding emission levels at the boundaries of ambient and driving conditions of the real-driving emissions (RDE) regulation. A Euro 6d-Temp GDI vehicle with a GPF was tested on the road and in the laboratory with cycles simulating congested urban traffic, dynamic driving, and towing a trailer uphill at 85% of maximum payload. The ambient temperatures covered a range from -30 to 50 °C. The solid PN emissions were 10 times lower than the PN limit under most conditions and temperatures. Only dynamic driving that regenerated the filter passively, and for the next cycle resulted in relatively high emissions although they were still below the limit. The results of this study confirmed the effectiveness of GPFs in controlling PN emissions under a wide range of conditions.

Keywords: vehicle emissions; cold start; low temperature; real-driving emissions (RDE); dynamic driving; regeneration; gasoline particulate filter (GPF)



Citation: Giechaskiel, B.; Valverde, V.; Kontses, A.; Melas, A.; Martini, G.; Balazs, A.; Andersson, J.; Samaras, Z.; Dilara, P. Particle Number Emissions of a Euro 6d-Temp Gasoline Vehicle under Extreme Temperatures and Driving Conditions. *Catalysts* **2021**, *11*, 607. <https://doi.org/10.3390/catal11050607>

Academic Editors: Maria Casapu and Dmitry E. Doronkin

Received: 21 April 2021

Accepted: 7 May 2021

Published: 10 May 2021

Publisher's Note: MDPI stays neutral with regard to jurisdictional claims in published maps and institutional affiliations.



Copyright: © 2021 by the authors. Licensee MDPI, Basel, Switzerland. This article is an open access article distributed under the terms and conditions of the Creative Commons Attribution (CC BY) license (<https://creativecommons.org/licenses/by/4.0/>).

1. Introduction

Air pollution has significant impacts on health, particularly in urban areas [1]. Air pollution, in particular $PM_{2.5}$ (particulate matter smaller than $2.5 \mu m$), is now clearly recognized as an important disease risk factor [2]. In 2019, exposure to $PM_{2.5}$ caused an estimated 7% of total global mortality and accounted for about 4.1 million deaths [2]. Studies have shown that exposure to high-average concentrations of $PM_{2.5}$ over the course of several years has been the most consistent and robust predictor of death from cardiovascular, respiratory, and other diseases [3]. Which component of PM is responsible for these adverse health effects is not clear. A review that examined the epidemiological and toxicological literature related to long-term exposure to PM found that, unlike the literature on short-term health effects, there is insufficient information to make clear judgments about the causal effects of PM components [4,5]. Nevertheless, there is increasing epidemiological evidence for an association between short-term exposure to ultrafine particles (smaller than $0.1 \mu m$) and cardiorespiratory health as well as the health of the central nervous system [6]. Ultrafine particles have a higher deposition fraction, deeper penetration, higher retention rate in the lungs, and the ability to migrate from the alveolar space into tissues and spread to organs such as the heart, liver, kidneys and brain [7].

Road transport contributes around 11% of PM_{2.5} emissions in the European Union (EU) [1], but the share is significantly higher in densely populated areas such as the Brussels–Capital Region, where it is 40% [8]. Lockdown measures in spring 2020 due to the SARS-CoV-2 virus led to small PM reductions in Europe [9], in some cases around 5–23% [10–12] but higher in Asia [13]. PM is predominantly caused by local meteorological conditions and regional transport. On the other hand, the particle number (PN) concentration is affected by local sources, especially combustion processes, of which a major contributor is vehicular exhaust [14].

Traditionally diesel-fueled vehicles have been the high PM emitters; however, with the introduction of diesel particulate filters (DPFs) emissions have decreased to the levels of gasoline vehicles. The requirement of low CO₂ emissions resulted in an increase in sales of gasoline direct-injection (GDI) vehicles as those are more fuel efficient than traditional port-fuel injection vehicles. The share of GDIs exceeded 50% in 2017 both in the EU and the United States and is still increasing [15]. The first GDIs had high PN emissions, one order of magnitude above the diesel PN limit of 6×10^{11} p/km [16]. In the EU, the introduction of a PN limit for GDIs resulted in low emission levels in the laboratory. The requirement to fulfil the limit on the road to meet the real-driving emissions (RDE) regulation practically forced the installation of gasoline particulate filters (GPFs) in most European GDIs [16], resulting in even lower PN emissions.

There are many published studies on GPF-equipped vehicles (e.g., [17–22]), many of which are summarized in the review [16]. Emissions are known to be low, especially after soot (or ash) accumulates in the particulate filter [23,24]. There are fewer studies at low ambient temperatures [19,25–27], but in general they confirm the effectiveness of GPFs in controlling PN emissions; however, information under challenging driving conditions is limited. For example, there is no published information on GPF-equipped vehicles during traffic congestion, high payload, dynamic driving, or high ambient temperatures.

The objective of this paper is to present the particle number emissions of a state-of-the-art Euro 6d-temp gasoline direct-injection (GDI) vehicle with a TWC (three-way catalyst) and GPF (gasoline particulate filter) under challenging conditions: extreme temperature (−30 to 50 °C) and in city traffic or under dynamic driving conditions.

2. Results

In this section, the initial type-approval test results are given. Then examples of real-time PN concentrations are presented followed by a summary of the PN emissions under various ambient temperatures and driving conditions. The details of the testing and instrumentation are given in Section 4 “Materials and Methods”.

2.1. Type-Approval Cycles

Figure 1 presents the PN emissions from the Type 1 worldwide harmonized light-duty vehicles test procedure (WLTP), with the relevant cycle (WLTC), and the Type 1A real-driving emissions (RDE) procedure following two routes on road (RDE road 1, 2). Furthermore, RDE-like cycles on the chassis dynamometer are included (not fully compliant with the RDE regulation) due to duration or ambient temperature (see Section 4.5).

The PN >23 nm WLTC emissions at 23 °C (3×10^9 p/km) were two orders of magnitude below the applicable Euro 6 limit (6×10^{11} p/km). The actual on-road tests at 17–20 °C, which complied with the RDE regulation (5×10^{10} p/km), were more than one order of magnitude below the not-to-exceed limit (9×10^{11} p/km). A short (1 h) RDE-like cycle conducted on the chassis dynamometer at 23 °C was also at similar levels (6×10^{10} p/km). Repeating the cycle at −10 °C did not increase emissions; actually, they were even lower (2×10^{10} p/km). Challenging the vehicle with a 2 h dynamic RDE cycle at −10 °C (RDE boundary) produced emissions still below the limit (1.4×10^{11} p/km). Tests at extreme temperatures (−30 and 50 °C) were also one to two orders of magnitude below the limit. The 5 °C test was higher than rest tests at different temperatures and similar to the RDE boundary test. This test will be discussed later.

The 10–23 nm particle concentrations were 16 to 38% of the >23 nm levels, except at $-30\text{ }^{\circ}\text{C}$, when it was 3.6 times higher but very low in absolute levels ($<1 \times 10^{11}$ p/km). Details will be given in the next sections.

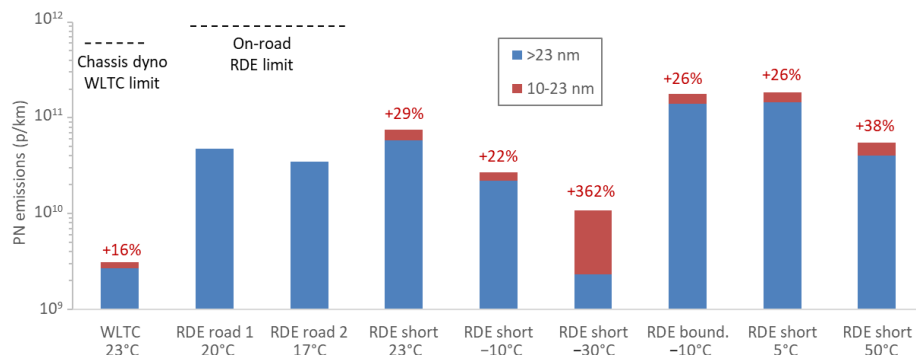


Figure 1. Particle number (PN) emissions for various cycles and ambient temperatures (in chronological order): Type 1 (WLTC), Type 1A on-road RDE (RDE road), RDE-like cycles tested on the chassis dynamometer (RDE short, RDE boundary). Dashed lines give the laboratory and on-road PN limits for this vehicle. RDE = real driving emissions; WLTC = worldwide harmonized light vehicles test cycle.

2.2. Real Time Examples

Figure 2 gives examples of PN >23 nm and >10 nm over short (1 h) RDEs at $23\text{ }^{\circ}\text{C}$ (Figure 2a) and $-10\text{ }^{\circ}\text{C}$ (Figure 2b). The emissions were higher during the first five minutes of the cold start then dropped to low levels with spikes only during acceleration. In general, the PN emissions followed the speed profile. The $-10\text{ }^{\circ}\text{C}$ test, other than a higher cold start spike, did not produce particularly higher emissions or different behavior. The PN >10 nm concentrations were around 28% higher than the >23 nm concentrations for both cycles and all parts of the cycle (urban, rural, motorway).

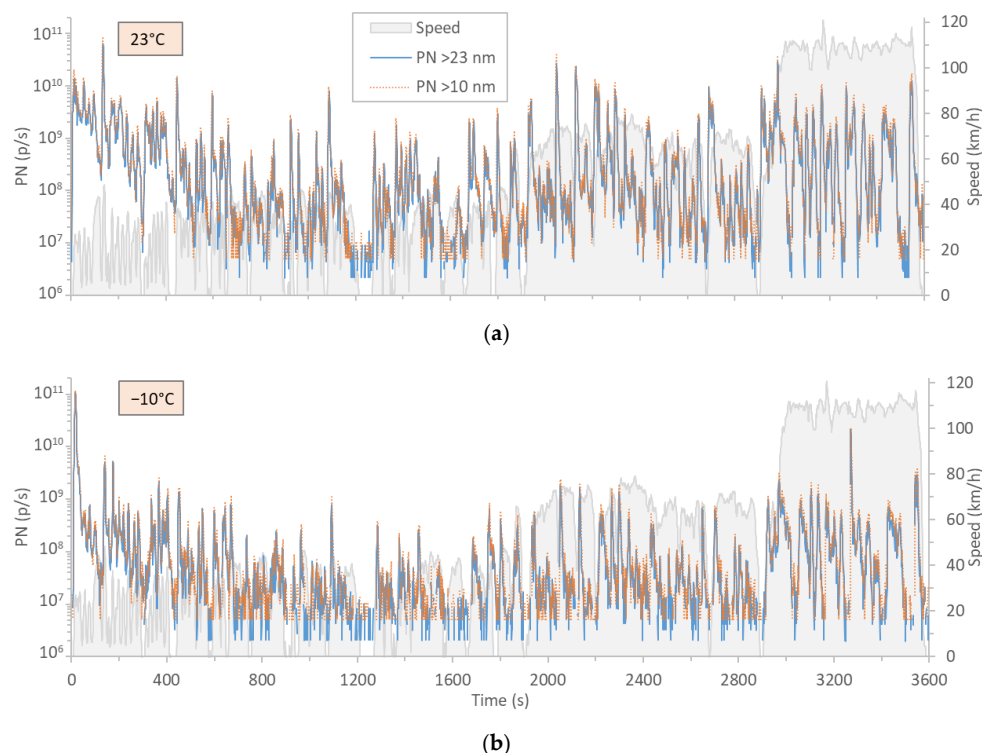


Figure 2. Short RDE driven on the chassis dynamometer: (a) Particle number (PN) > 23 (blue line) and >10 nm (orange line) at $23\text{ }^{\circ}\text{C}$, and; (b) $-10\text{ }^{\circ}\text{C}$. The speed profile is given in grey background.

Figure 3 presents the PN >23 nm and >10 nm emissions over the city cycle TfL (Transport for London) followed by the dynamic motorway cycle BAB (Bundesautobahn) at -30 , 5 , and 50 °C. As previously mentioned, after the cold-start emissions, PN levels remained at low levels (10^7 p/s) at -30 °C (Figure 3a), and spikes could later be seen during the hard accelerations (reaching 10^{10} p/s) during the BAB cycle, which far exceeded the dynamicity limit ($v \times a$) of the RDE regulation. Nevertheless, the emissions were very well controlled. The sub-23 nm particle concentrations were relatively elevated only at the beginning of the test at -30 °C. During the first two minutes, the >10 nm concentration was 15% higher than the >23 nm concentration (until 140 s), and then for the next four minutes (140–400 s) was 190% higher.

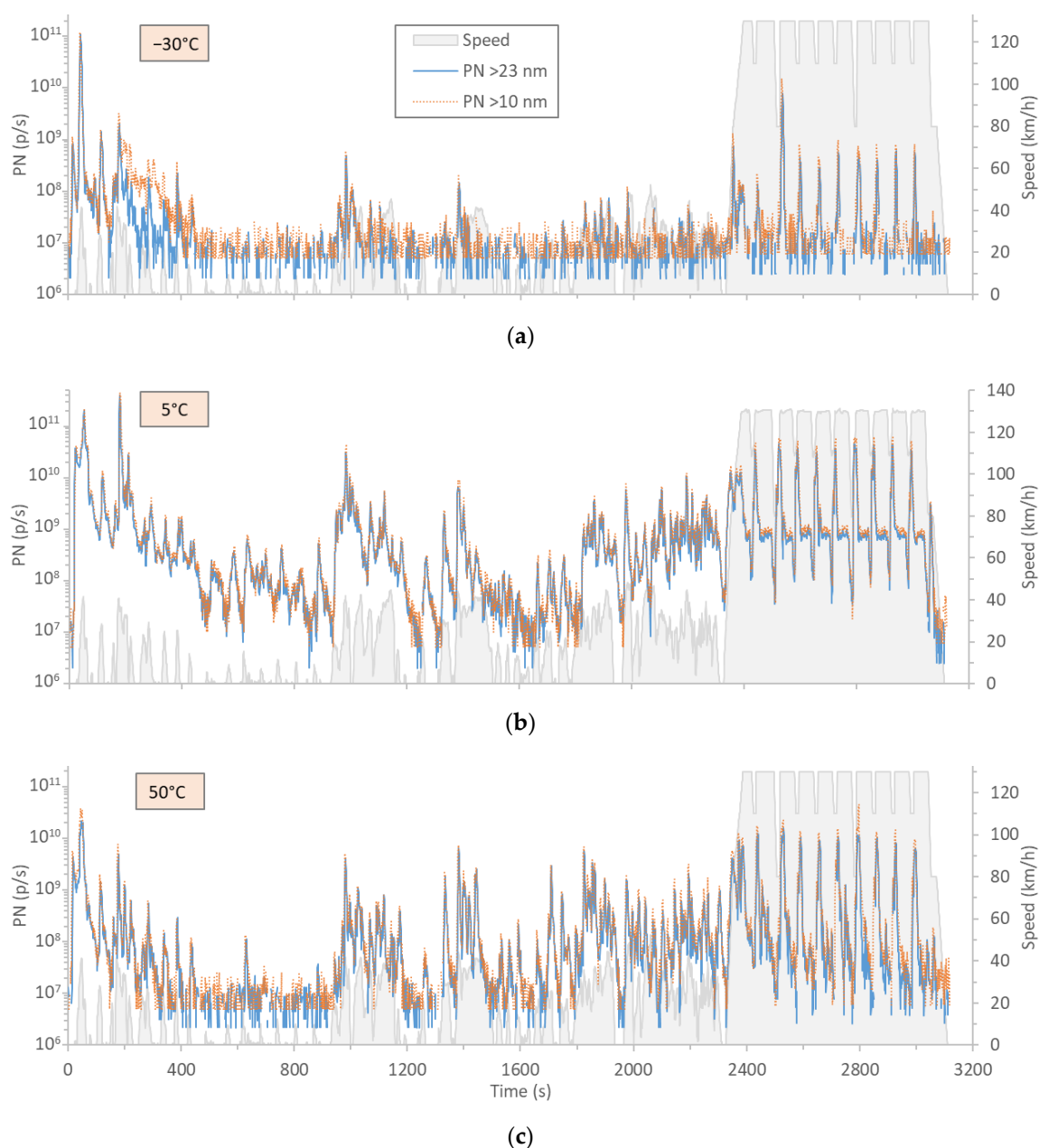


Figure 3. Urban cycle TfL and motorway BAB driven on the chassis dynamometer: (a) Particle number (PN) > 23 (blue line) and >10 nm (orange line) at -30 °C; (b) 5 °C, and; (c) 50 °C. The speed profile is given in grey background.

Surprisingly, emissions at 5 °C (Figure 3b) were much higher compared to those at -30 °C and other temperatures as will be shown later. The PN signals clearly followed

the speed profile. As was previously the case, emissions were higher during the cold start, and spikes appeared during accelerations. Compared to the $-30\text{ }^{\circ}\text{C}$ test, the emissions were elevated by more than one order of magnitude (see BAB baseline 7×10^9 p/s at $5\text{ }^{\circ}\text{C}$ vs. 1×10^7 p/s at $-30\text{ }^{\circ}\text{C}$). The PN >10 nm emissions were 20–40% higher than the PN >23 nm emissions over this test.

The $50\text{ }^{\circ}\text{C}$ test (Figure 3c) had emissions slightly higher than at $-30\text{ }^{\circ}\text{C}$, but much lower than at $5\text{ }^{\circ}\text{C}$. The PN >10 nm emissions were around 50% higher than the >23 nm emissions.

In order to better understand the previous results, Figure 4 presents the cycle that was driven between the two tests of -30 and $5\text{ }^{\circ}\text{C}$: a 2 h dynamic RDE cycle at $-10\text{ }^{\circ}\text{C}$ (RDE boundary). The $50\text{ }^{\circ}\text{C}$ cycle was driven after the $5\text{ }^{\circ}\text{C}$ test (see details in Chapter 4). Figure 4a shows the urban part, while Figure 4b shows sections of all three parts (urban, rural and motorway). The RDE cycle was very dynamic with $v \times a$ values at the limits of RDE regulation or slightly higher. This was evident from the speed profile, which consisted of hard acceleration and braking. The cycle was artificial and the driving was atypical and resulted in considerable tire wear. Due to the highly dynamic conditions of this test, it was assumed that the GPF was passively regenerated. Thus, the filter was relatively clean in the follow-up test (RDE at $5\text{ }^{\circ}\text{C}$) and resulted in elevated emissions.

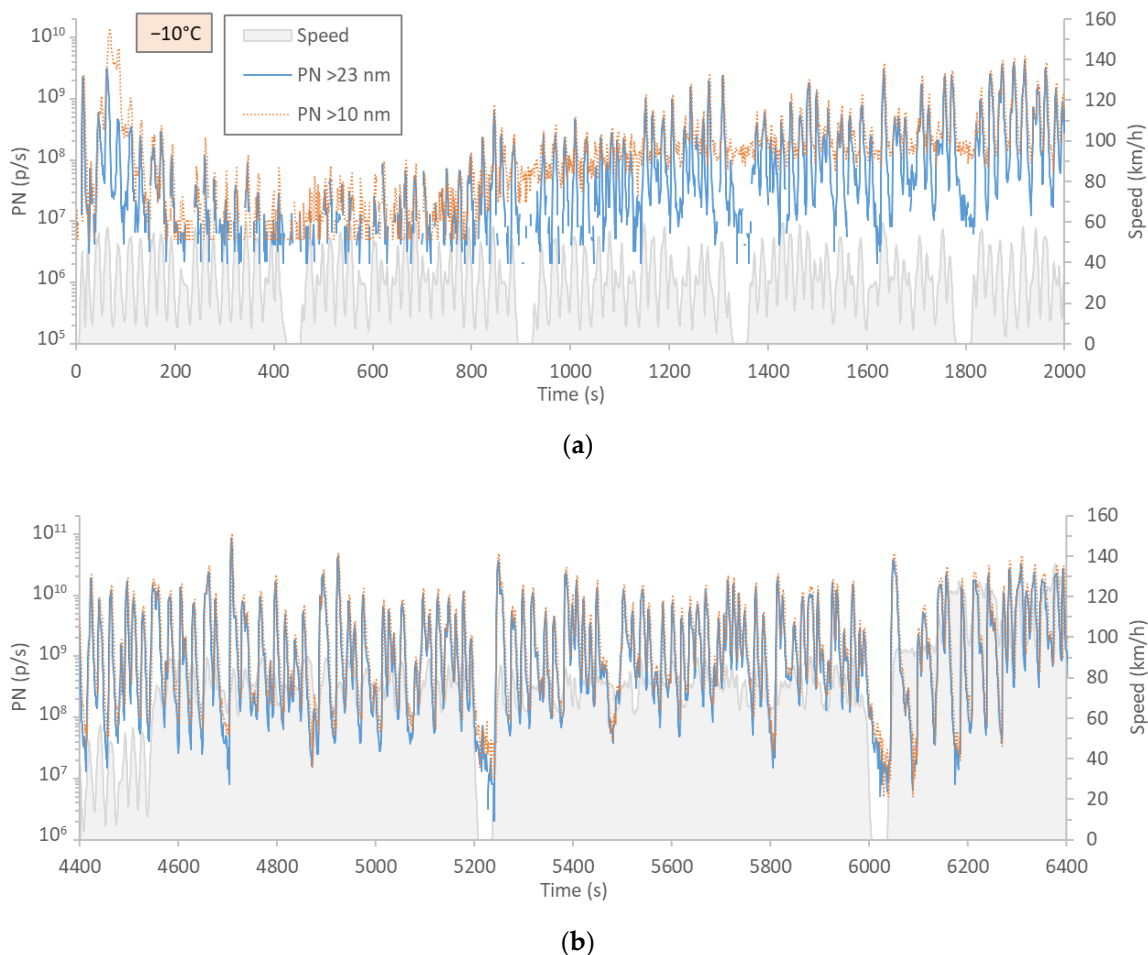


Figure 4. Particle number (PN) >23 (blue line) and >10 nm (orange line) over sections of the dynamic RDE cycle at the boundaries of the RDE dynamicity limits (RDE boundary) driven on the chassis dynamometer at $-10\text{ }^{\circ}\text{C}$: (a) urban section and; (b) parts of the urban, rural, and motorway sections. The speed profile is given in grey background.

As Figure 4a shows, emissions were low (PN >23 nm 10^7 p/s) 200 s after the cold start, but started to increase at 800 s. At approximately 1800 s, the emission levels stabilized at a higher level (PN >23 nm 10^8 p/s). The sub-23 nm particle concentration was high at

the cold start (4.5 times higher for the first 3 min), low afterwards (65% until 800 s) and then high at the idle or deceleration (average 50% after 800 s).

Continuing with Figure 4b (note the different PN *y*-axis scale), urban, rural, and motorway PN > 23 nm emissions were high, ranging from 10^9 p/s to 10^{10} p/s and followed the speed profile. The concentration of sub-23 nm particles was not particularly high (26–32%).

2.3. Urban Emissions

Figure 5 summarizes PN emissions for the urban cycles (TfL, uphill) and urban parts of the rest cycles (RDE short, RDE boundary, RDE road, WLTC). The distances were 9–12 km, with the exception of the dynamic RDE boundary and actual RDE on-road cycles, where the urban distances were around 36 km. The emissions for the urban part of the RDE boundary cycle are also given for the first 10 km. Details for the cycles are given in Section 4 “Materials and Methods”.

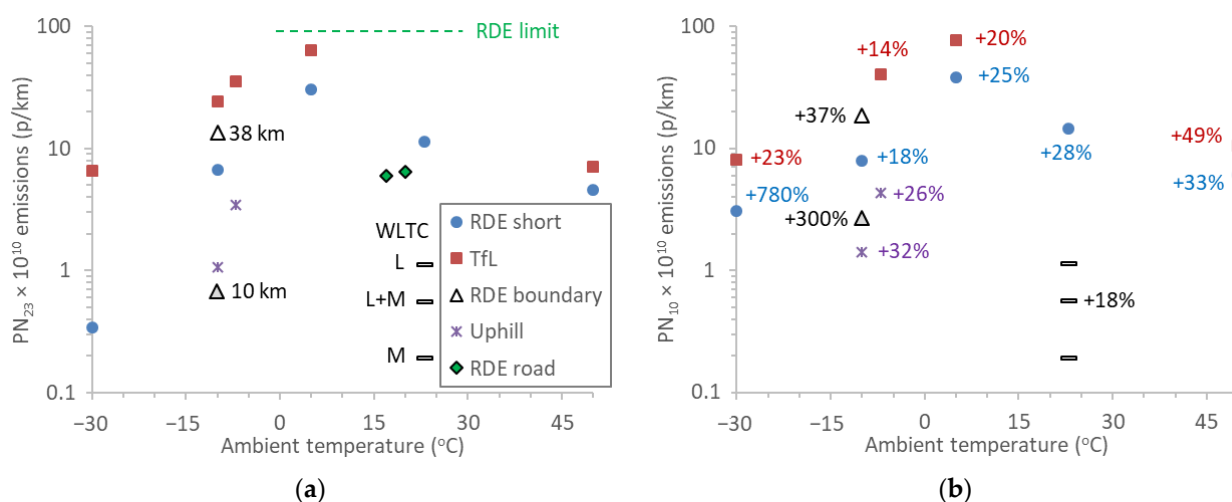


Figure 5. Particle number (PN) emissions of urban cycles (TfL, Uphill) or urban parts of the rest cycles (RDE short, RDE boundary, RDE road, WLTC) in function of ambient temperature. The emissions of the low (L) and medium (M) parts of the WLTC are also given. (a) PN > 23 nm; (b) PN > 10 nm. Percentages give the excess particles between 10 nm and 23 nm. RDE = real-driving emissions; WLTC = worldwide harmonized light vehicles test cycle.

For the urban tests, the only applicable limit is the on road RDE limit of 6×10^{11} p/km with conformity factor of 1.5. The conformity factor takes into account the PEMS uncertainty [28], which normally should not be applied for the chassis dynamometer tests, where laboratory-grade equipment was used. It should be noted that for extended conditions (temperature 0–7 or 30–35 °C, altitude >1300 m), a correction factor of 1.6 had to be applied to the emissions, or equivalently the limit would have been 1.6 times higher. For temperatures <−7 or >35 °C, the test is not RDE compliant. We did not apply the conformity factor and the extended conditions correction factor to our result. The PN emissions were much lower than 6×10^{11} p/km under all temperatures (note the logarithmic *y*-axis scale), with one exception at 5 °C which was close to the PN limit. It should be mentioned that no limits were applicable to the specific cycles because they were not RDE compliant (e.g., the distance was shorter than 16 km, and for some of the cycles the ambient temperature was outside the boundaries).

In general, there was no clear trend in PN emissions as a function of temperature or cycle. The PN >23 nm emissions were $>1 \times 10^{11}$ p/km at the −7, −10, and 5 °C TfL; the 5 °C urban RDE cycle; and the −10 °C dynamic RDE boundary test. As mentioned before, the 5 °C tests were conducted after the dynamic RDE (RDE boundary) test, which probably regenerated the filter. Consequently, the 5 °C tests were run with a relatively empty filter

and the emissions were higher. The Tfl cycles had high cold-start emissions which resulted in relatively high emissions due to the short distance of the cycle.

The percentages of sub-23 nm were between 14 and 49%. One exception was the RDE boundary for the first 10 km, where the percentage was 300%, and the RDE short at $-30\text{ }^{\circ}\text{C}$. In both cases the $>23\text{ nm}$ emissions were $<7 \times 10^9\text{ p/km}$.

2.4. Motorway Emissions

Figure 6 summarizes the PN emissions for the motorway cycle BAB and the motorway parts of the RDE cycles or WLTC. All motorway cycles were with hot engine. The cycles were 19 km (RDE short) to 34 km (RDE road) long, with the exception of the extra high part of the WLTC (8.3 km long).

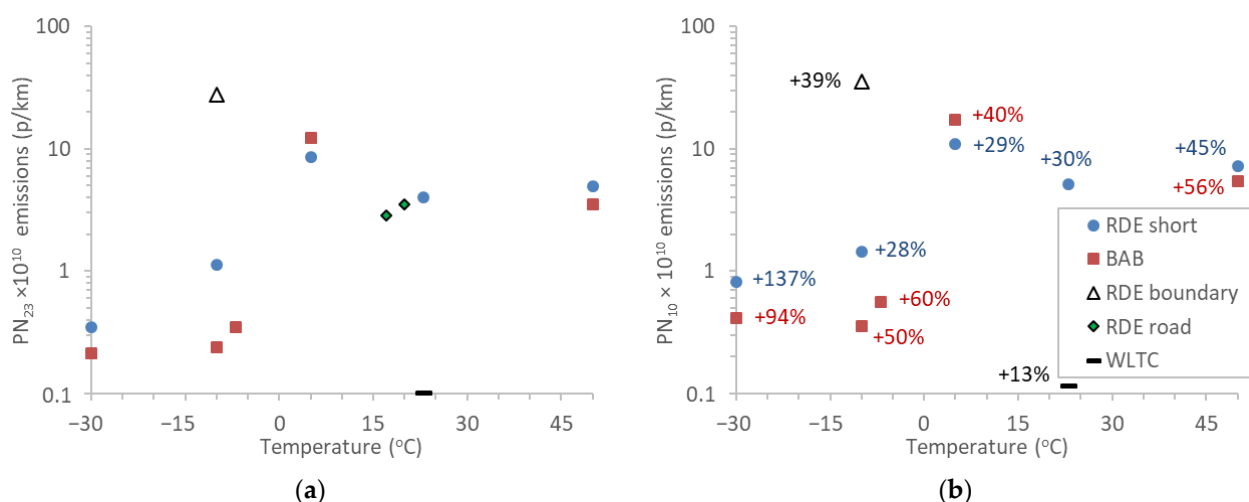


Figure 6. Emissions of motorway cycle (BAB) or motorway parts of the rest cycles (RDE short, RDE boundary, RDE road, WLTC) in function of ambient temperature. The emissions of the extra-high part of the WLTC are also given. (a) PN $> 23\text{ nm}$; (b) PN $> 10\text{ nm}$. Percentages give the excess particles between 10 nm and 23 nm. RDE = real-driving emissions; WLTC = worldwide harmonized light vehicles test cycle.

There was a small tendency toward higher emissions with higher ambient temperatures. The $5\text{ }^{\circ}\text{C}$ tests were above the trendline for the reason discussed previously: the filter was empty and the emissions relatively higher. Higher emissions were also noted for the dynamic RDE boundary ($1.4 \times 10^{11}\text{ p/km}$).

The sub-23 nm fraction was 28 to 60%. Higher percentages were measured at the $-30\text{ }^{\circ}\text{C}$ motorway tests (94–137%), but the $>23\text{ nm}$ emissions were low in absolute levels $<4 \times 10^9\text{ p/km}$.

3. Discussion

This study assessed the particle number (PN) emissions of a gasoline direct-injection vehicle equipped with a three-way catalyst and a gasoline particulate filter (GPF). In addition to the type-approval cycles (WLTC and on-road RDE), various RDE-like, city (urban) and highway (motorway) cycles were tested over a wide range of temperatures.

The vehicle emissions were well below the applicable PN limits for laboratory type 1 (WLTC) and type 1A on road RDE cycles. The limits were also respected under all tested cycles, temperatures, and driving conditions even though it was not applicable. The results of this study confirmed the efficiency of GPFs for controlling PN emissions under a wide range of ambient and driving conditions. Relatively high emissions were measured during cold starts and accelerations. Furthermore, the levels were generally elevated after the dynamic cycle, which probably regenerated the GPF. These topics will be discussed in the following paragraphs.

The cold start emissions showed the typical behavior of vehicles with particulate filters: high emissions at the beginning and decreasing after a few minutes [20]. When a cold engine starts, excess fuel must be supplied to assure enough fuel vapor to create a combustible gas mixture [29]. Enriching the air-fuel mixture, along with other methods such as retarded spark timing, higher idle speeds, and artificial loading of the engine, are also used to increase the exhaust temperature and decrease the catalyst light-off time [30,31]. Because cold engine parts (cylinder walls, piston crown and parts of the fuel system), have a negative effect on fuel evaporation and mixture enrichment, they lead to a heterogeneous charge and localized fuel-rich regions, thus creating higher engine-out emissions [29,32]. Why these solid particles are filtered with low-filtration efficiency only during the first minutes of a cold start has not been discussed in detail. One explanation is that these solid particles are heavy hydrocarbons or polycyclic aromatic hydrocarbons (PAHs) from the pyrolysis of incompletely combusted larger fuel fragments and oil lubricant [33–36] that did not evaporate during the thermal pretreatment of the PN system (heated to 350 °C). In addition to higher engine-out emissions [37,38] and higher amounts of semi-volatile and non-volatile particles, other mechanisms have been suggested to explain the high cold-start PN emissions. These include small leaks between the mat and the canister that closes as the filter heats up [25], cracks in the soot cake that occur during cooling, small soot particles in the interstices of the substrate that are blown about when the exhaust flow starts [39], and fragmentation of pre-deposited soot [39,40]. It has also been suggested that the filtration efficiency is lower at urban conditions due to a lower exhaust flow rate and resulting particle diffusion [29,41]. Quite often at a cold start, high concentrations of large particles having a lower filtration efficiency than smaller ones are emitted [37].

Previous studies showed that low ambient temperatures result in high PN emissions in GDI vehicles without GPF [16,38,42–46] and with GPF [19,25–27] when tested with cycles that include a cold start. Low ambient temperatures can increase the contribution of unburnt fuel to particulate emissions, as one study with older vehicles showed [47]. The GPF-equipped vehicle in our study showed a very good control of PN emissions at low ambient temperatures. After the cold start parts, PN emissions were almost independent of the ambient temperatures for the duration of the cycles, as others have also noted [27]. It is likely that the high engine-out emissions at low temperatures made the GPF loading faster and improved filtration efficiency (see results of the –30 °C test, after the –10 °C, e.g., Figure 1). A study with urban driving of 6 km with <30 km/h speed, found a soot loading rate 0.02 g/L at 0 °C to 0.2 g/L at –30 °C [48].

Interestingly, uphill driving produced emissions more than one order of magnitude below the limit. One of the tests (–7 °C) was conducted with an 85% payload of the car and trailer. Like the rest of the cold start cycles, the majority of the particles were emitted during the first minutes. Due to the smooth accelerations of the cycle, the emissions were very low and the very high payload had no influence. This finding is important considering that the engine-out emissions typically increase with engine load (power) [49].

At high engine speed and load, air/fuel enrichment for thermal component protection takes place. The resulting lack of oxygen and high temperatures promotes the formation of particulate matter, so the PN concentration rises [29]. In our study, emissions were kept low even at high speeds with the exception of accelerations. However, a trend toward higher emissions with increasing ambient temperature was evident in the motorway cycles. High emissions during acceleration is known [41,49–51], and in previous studies, dynamic driving doubled the PN emissions [19,26].

The sub-23 nm fraction was generally low (14–49% for urban cycles, 28–60% for motorway cycles), which was in agreement with previous studies [16,21,29,34,41,52–55]. However, we noticed a high sub-23 nm fraction in cold starts during low ambient temperature tests (exceeding 300%). Others have reported high sub-23 nm particle concentrations at idle and low coolant temperatures [56], which could be caused by incomplete combustion and high amounts of unburnt fuel. Dynamic urban driving resulted in PN spikes and braking and decelerating showed high sub-23 nm fractions. Other researchers have been

attributed these particles to particles of oil lubricant [57]. Nevertheless, absolute urban PN emissions >23 nm of specific cycles were low ($<7 \times 10^9$ p/km; Figure 5a). Urban 10–23 nm emissions were in most cases $1\text{--}5 \times 10^{10}$ p/km.

At high engine speeds, increases in the sub-23 nm fraction from increased oil consumption or worn piston ring sealing was reported [58]. In other studies [29], as well ours, this was not so evident: the sub-23 nm percentages were only slightly higher (28–60% vs. 14–49% of urban cycles). This was probably because the piston rings sealed the combustion chamber properly, resulting in a negligible amount of lubricant consumption during combustion. Furthermore, good filtration efficiency might have masked any increase of engine-out emissions.

The results also showed that absolute PN levels depended on the fill state of the filter. High emissions were noted for the cycle run at 5 °C after the dynamic test as previously discussed. The emissions were higher because the GPF was relatively empty. GPFs passively regenerate continuously, thus the fill state remains at similar levels. However, the soot-burning rate depends on oxygen availability and exhaust gas temperature [59]. We noted a big difference only during the dynamic cycle when emissions increased. It is likely that the high exhaust gas temperature resulted in high soot-burning rates. A study found conditions suitable for regeneration (defined in their study as exhaust gas temperature >500 °C and oxygen concentration >5%) around 12% during WLTCs, but 15–27% during aggressive cycles, which supported our assumption [60]. In our dynamic cycle, very frequent braking increased oxygen availability. The oxygen availability is important because uphill driving, even with the 85% payload of car and trailer, did not regenerate the filter because of a high exhaust gas temperature. Such high emissions during passive regeneration were also noted by another study [40,61]. Substantial amount of semi-volatile material was likely generated by the incomplete combustion of accumulated soot in the GPF during regeneration [62]. It was also suggested that during filter regeneration, incipient soot particles may be generated from the volatile and semi-volatile hydrocarbon species formed by incomplete soot oxidation [62]. The contribution of thermally desorbed and pyrolyzed materials (e.g., heavy hydrocarbons, ash, and inorganic salts) deposited in the exhaust pipe, catalytic converter, and muffler provide an additional particulate matter source not present during moderate driving and cannot be excluded for the specific dynamic test [40,63]. However, such desorption phenomena would not be able to explain the high emissions during the 5 °C test because the exhaust gas temperature was lower. It should also be highlighted that the differences of the emissions with an empty GPF were almost 10 times higher compared to the “normal” load, indicating that GPFs with high efficiency could be important depending on the engine-out emissions. It should also be added that the RDE boundary was artificial and not representative of real aggressive driving; thus, it could be that the GPF would never regenerate to such levels. The key message is that vehicle pre-conditioning can be important for GPF-equipped vehicles. In the case of diesels, emissions immediately after regeneration can be two orders of magnitude higher than before [64].

Even though it was clear that PN emissions were produced during acceleration, the correlation between PN emissions and the dynamicity index 95th percentile of $v \times a$, did not reveal any trends. Figure 7a plots the correlation of the urban cycles, while Figure 7b does so for the motorway cycles. As discussed previously, for urban cycles the contribution of a cold start (and ambient temperature) and total distance were the more important parameters. For the motorway cycles, the GPF fill state was of higher importance. These results suggested that for GPF-equipped vehicles the dynamicity index is not so important or a different index could be more useful. Other metrics have also been suggested by others [65], and this is a topic that needs further investigation, in particular after consideration of gaseous pollutants [66].

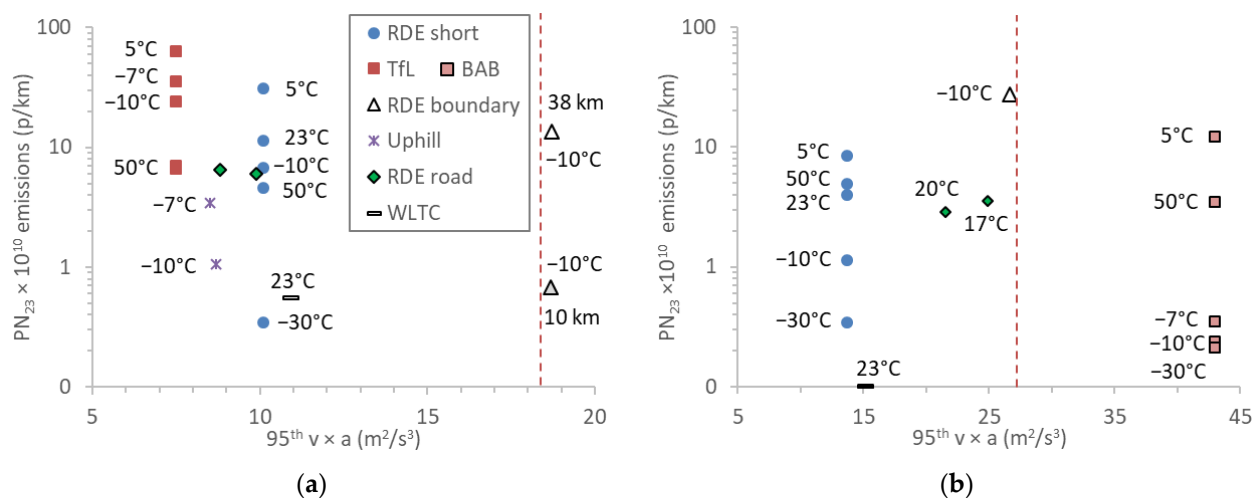


Figure 7. Particle number (PN) emissions > 23 nm in function of dynamicity expressed as 95th percentile of $v \times a$ of (a) urban cycles (TfL, Uphill) or urban parts of the rest cycles (RDE short, RDE boundary, RDE road, WLTC); (b) motorway cycle (BAB) or motorway parts of the rest cycles (RDE short, RDE boundary, RDE road, WLTC). Dashed lines show approximate dynamicity limits which depend on the mean speed. RDE = real-driving emissions; WLTC = worldwide harmonized light vehicles test cycle.

In closing, the tests were conducted with the odometer at approximately 24,000 km. It is known that the GPF performance improves with mileage [23,24,29]. Indeed, our WLTC results were much lower than those reported in the certificate of conformity (CoC) of the vehicle (typically conducted with very low mileage). Nevertheless, durability issues, such as cracks or damages need to be checked when approaching the end of its useful life (currently set in Regulation (EC) 715/2007 at 160,000 km). On the contrary, it has been reported that GPFs are robust up to temperatures of 1100 °C and the filtration efficiency increases after 20,000 km [67]. In another study the filtration efficiency reached 99.7% after an equivalent aging of 200,000 km [68]. Finally, the effect of fuel, which might be important [69–71] was not investigated as all tests were conducted with the same market fuel (E10). A study found a factor difference of 5 among market fuels and 10 among market and certification fuels [72]. Finally, the effectiveness of GPFs has to be assessed under future Euro 7 limits. The final proposal is expected in 2022, but the proposal of CLOVE (Consortium for ultra LOW Vehicle Emissions), tasked by the European Commission to give guidelines for the upcoming Euro 7 emission standards, suggested a limit of 1×10^{11} p/km for a distance of 16 km. The first morning cycle after the dynamic test had emissions of 6×10^{11} p/km (TfL), while the urban part of the evening cycle had emissions of 2×10^{11} p/km (RDE short); thus, only 9 km of driving with the TfL cycle resulted in a soot load high enough to improve significantly the filtration efficiency. Nevertheless, these results highlight the need of the latest generation GPFs, which deliver >90% filtration efficiency “out of the box” (i.e., low mileage <200 km) [73].

4. Materials and Methods

4.1. Instrumentation

The test campaign was carried out in the European Commission’s Joint Research Centre (JRC) vehicle emissions laboratory (VELA 8); a chassis dynamometer test cell with controlled temperature and relative humidity. The four-roller dynamometer was set in rear-wheel drive—forward synch mode, so that both rear (powered) and front (non-powered) axles rotated synchronously. For all tests conducted, regulated gaseous emissions were measured in the full dilution tunnel in real-time with an AMA i60 bench (AVL, Graz, Austria). Solid particle number emissions from approximately 23 nm were measured with an advanced particle counter (APC 489) (AVL) [74] connected to the full dilution tunnel. The system included an evaporation tube at 350 °C to remove volatiles. A 3010 condensation particle

counter (CPC) (TSI, Shoreview, MN, USA) connected to the APC measured particles from approximately 10 nm. The emissions were calculated as with the 23 nm counter (i.e., using the mean particle concentration reduction factor of 30, 50, and 100 nm, as suggested in the future regulation: UNECE global technical regulation 15). This meant that the losses in the 10–23 nm region were not taken into account (approximately 50%) [20]. Consequently, the 10–23 nm concentrations reported were underestimated by a factor of two (i.e., the 10–23 nm percentages reported can be multiplied by two to get the “true” concentration). Details can be found elsewhere [20]. A thermocouple was used to measure the temperature at the tailpipe.

4.2. Vehicle and Fuel

The test vehicle was a 2019 model-year (Euro 6d-Temp-Evap-ISC), direct-injection gasoline passenger car with a 135 kW four-cylinder, in-line 2.0 L engine, with a close-coupled three-way catalyst (TWC) and an underfloor uncoated gasoline particle filter (GPF) as emissions controls. A vehicle rental company sourced the vehicle. Gasoline (E10) market fuel was used for all tests. The odometer reading at start of the test campaign was 24,130 km. The vehicle air conditioning (A/C) system was used and set at a temperature of 21.5 °C for all tests. No other auxiliary system was used on any test (no defrost function).

Prior to the start of the test, the vehicle was physically checked and no anomalies or malfunctioning was identified. An on-board diagnostics (OBD) scan was also performed on modalities 3/7/A and 9 and showed no errors.

4.3. Test Cycles

The vehicle was driven on a variety of driving cycles that aimed to reproduce standard as well as challenging driving situations (see also Figure 8, Tables A1–A3 (Appendix A)).

- WLTC: The type 1-approval cycle: worldwide harmonized light-vehicle test cycle (WLTC).
- TfL: The Transport for London urban interpeak (TfL) cycle represented urban driving characterized by stop-and-go traffic under congested conditions.
- BAB: From the German *Bundesautobahn*, (“federal highway”), the BAB 130 cycle represented high-speed motorway driving up to 130 km/h with frequent and sharp acceleration from 80 to 130 km/h and from 110 to 130 km/h.
- RDE short: The short real-driving test (RDE) was a 1 h test that reproduced an on-road test on the dyno with a time share of 53% urban driving, 28% rural, and 19% motorway with a road slope ranging from −9.6 to 9.2%. The distance shares were 34%/30%/36%.
- RDE boundary: A 2 h on-road test on the dyno used a speed profile that recreated the most dynamic drive possible within the RDE boundaries of speed times acceleration, with 90% payload (RDE boundary). The urban/rural/motorway time shares were 65%/20%/15%, and the distance shares were 38%/30%/32%.
- Uphill: An uphill-only driving cycle (speed <60 km/h) was used involving modified dyno loads to simulate (i) towing a 800 kg trailer on a 5% constant slope (uphill tow) and (ii) driving on a 5% constant slope loaded to 85% payload capacity and towing a 1700 kg trailer (85% of maximum trailer weight) (uphill tow 85%).
- RDE road: The type 1A-approval on-road test (RDE road). Two different RDE compliant routes were tested. These tests were conducted on the road with portable emissions measurement system (PEMS), in contrast to the rest tests, which were conducted on the chassis dynamometer. The PEMS was the MOVE from AVL based on diffusion charging for counting particles [28]. The system included a catalytic stripper at 300 °C to remove volatiles.

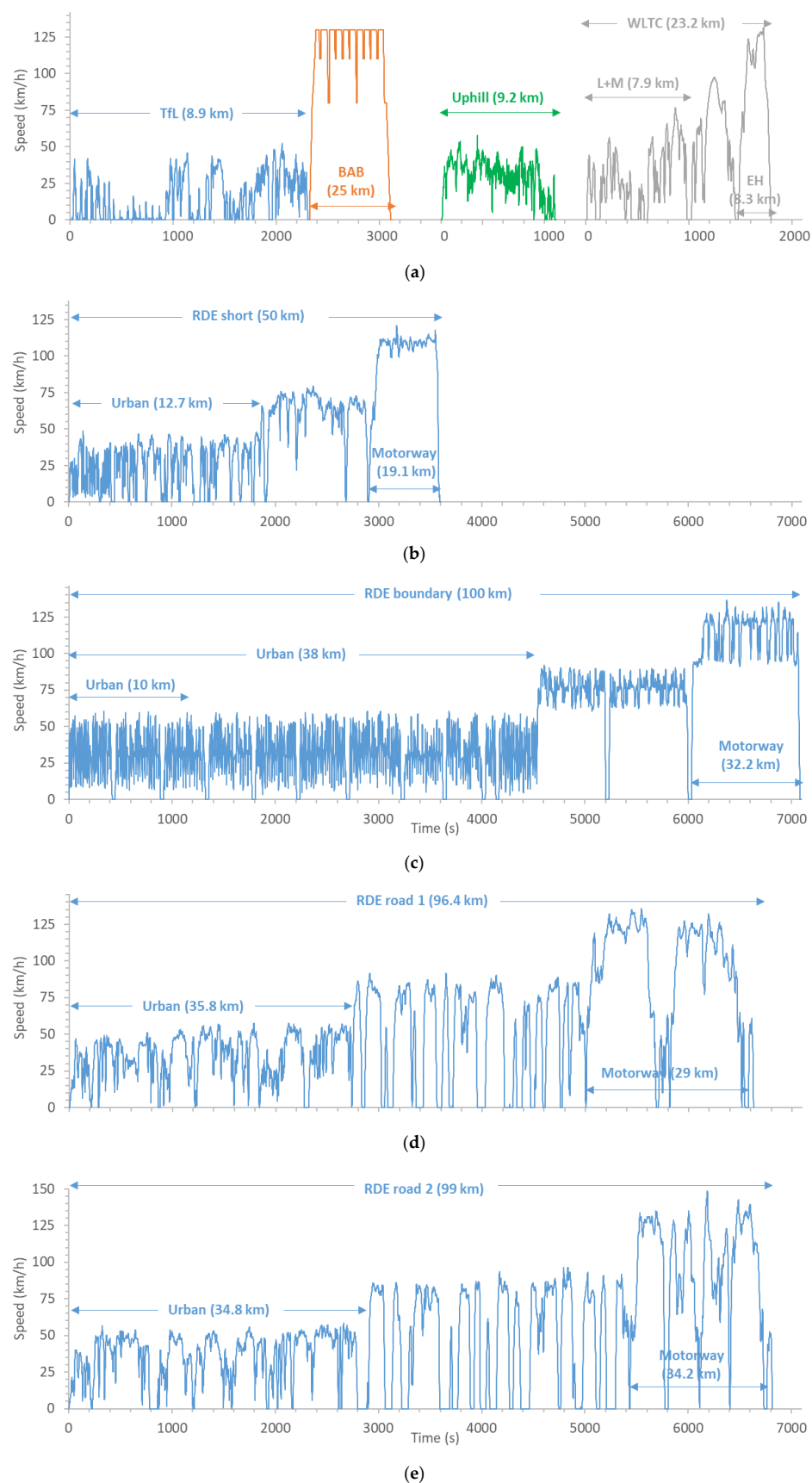


Figure 8. Cycles: (a) TfL, BAB, uphill, WLTC; (b) short RDE (c); RDE boundary; (d) RDE on-road 1; (e) RDE on-road 2. The division in urban, rural and motorway parts is also shown. Cycles “road 1” and “road 2” were driven on the road, while the rest were conducted on the chassis dynamometer.

All cycles conducted on the chassis dynamometer, except the BAB, were tested with an engine cold start, i.e., soaked at the temperature of the dyno for the specific test (i.e., between -30 and 50 °C). The soaking of the vehicle before the on-road tests was done at a soaking area of approximately 17 – 20 °C.

The WLTC tests were conducted using the test mass and the road-load coefficients declared on the CoC (Certificate of Conformity), after road-load derivation on the dyno. For the rest cycles, the test mass and the dyno coefficients were adjusted depending on the simulated conditions (e.g., slope, extra weight). Road-load coefficients (F2) were not increased by 10% at sub- 0 °C temperatures. Details can be found in Tables A1–A3. For driving dynamics, the RDE boundary motorway part was at the 95th $v \times a$ limit ($26.8 \text{ m}^2/\text{s}^3$), while the motorway cycle BAB exceeded it. The RDE boundary urban part exceeded the 95th $v \times a$ limit ($18.5 \text{ m}^2/\text{s}^3$), but was below when considering the whole cycle, as it would be done at the RDE evaluation.

4.4. Test Protocol

Each day, two cold-start tests were performed (Table 1). The morning test (TfL followed by BAB) was preceded by an overnight soaking period of about 12 h at the test temperature. The soaking between the morning and evening tests was about 5 h and forced cooling was applied before the evening test (i.e., fan at 60 km/h with the engine compartment cover open). The evening test was usually the RDE short cycle. Based on coolant and exhaust gas temperatures (Figures A1 and A2), and the trends on PN emission levels from morning and evening tests, we assumed that the forced cooling would sufficiently cool down the GPF. No other vehicle was tested in the laboratory during this period. A 12 V battery was charged prior to each test of the campaign at the ambient temperature of the forthcoming cycle. The ambient temperatures tested were -30 , -10 , -7 , 5 , 23 , and 50 °C.

Table 1. Test protocol.

	Day 1	Day 2	Day 3	Day 4	Day 5	Day 6	Day 7	Day 7	Day 8
Place	Road	Lab	Lab	Lab	Lab	Lab	Lab	Lab	Lab
Temp.	17 – 20 °C	23 °C	23 °C	-10 °C	-30 °C	-10 °C	5 °C	50 °C	-7 °C
Morning	RDE road 1	WLTC	TfL + BAB	TfL + BAB	TfL + BAB	Uphill tow	TfL + BAB	TfL + BAB	TfL + BAB
Evening	RDE road 2	WLTC	RDE short	RDE short	RDE short	RDE boundary	RDE short	RDE short	Uphill tow 85%

A value of 45% relative humidity was chosen for the positive temperature tests since this was appropriate for regulated measurements at 23 °C. The temperatures -30 and 50 °C were selected for testing because any optimized calibration from the OEM (original equipment manufacturer) is unlikely. Note that such temperatures are not expected in Europe; hence, the vehicle is not expected to comply with any EU limits.

4.5. RDE Compliance

None of the laboratory RDE-like cycles were Euro 6d RDE compliant. The RDE short was only 1 h long (RDE requires 1.5–2 h) and the urban distance was 12.7 km (RDE requires >16 km). The tests at -30 , -10 , and 50 °C were outside the RDE temperature boundaries (-7 to 35 °C). The RDE boundary cycle had an urban 95th $v \times a$ of $18.7 \text{ m}^2/\text{s}^3$, which is higher than the RDE limit of $18.5 \text{ m}^2/\text{s}^3$. Furthermore, it was run at -10 °C, which is outside the RDE lower temperature boundary of -7 °C. The TfL was the only urban cycle with distance of 8.9 km (RDE requires >16 km). As with the RDE short cycle, the TfL tests at -30 , -10 , and 50 °C were outside the temperature boundaries (-7 to 35 °C). The uphill cycles were not compliant because they simulated towing a trolley with 40–85% of the trolley maximum payload (RDE does not allow towing a trolley). In addition, one of the uphill tests, at -10 °C, was outside the RDE temperature boundaries. The BAB was the motorway cycle with a 95th $v \times a$ of $43.5 \text{ m}^2/\text{s}^3$, which exceeded the RDE limit of

27.3 m²/s³. Furthermore, the tests at −30, −10, and 50 °C were outside the temperature boundaries (−7 to 35 °C).

At the moment there is no official proposal from the European Commission regarding Euro 7. Based on the CLOVE proposal, the boundaries will not be fundamentally different [75]. For example, the reference distance will be kept at 16 km, but allowing shorter trips the suggested temperature range is −10 to 40 °C. Dynamic driving over a trip is still under discussion, and alternative indicators are under consideration.

5. Conclusions

A Euro 6d-temp gasoline vehicle with TWC (three-way catalyst) and GPF (gasoline particulate filter) was tested on the road according to the type 1A on-road real-driving emissions (RDE) procedure at 17–20 °C and in a laboratory according to the type 1 worldwide harmonized light-vehicles test procedure (WLTP) at 23 °C. Additional urban, motorway, dynamic, and uphill-driving cycles with different payloads were conducted in the laboratory at temperatures between −30 and 50 °C.

The particle number (PN) emissions were below the limit under all driving conditions, confirming the effectiveness of the GPF. Emissions close to the limit were measured at the cycles after the dynamic RDE test. It was assumed that the GPF would passively regenerate during the dynamic cycle and that the emissions would be high at the subsequent cycles due to the decreased filtration efficiency, thereby highlighting the importance of vehicle preconditioning. Relatively elevated emissions were measured during the cold start and cycles that included strong accelerations. There was also some evidence that driving at very low temperatures increased GPF soot loading and had a favorable effect on filtration efficiency. No particular trend was observed in function of ambient temperature or dynamicity expressed as the 95th percentile of speed times acceleration, an index prescribed in the RDE regulation. The sub-23 nm fraction was around 14–60% depending on the cycle and ambient temperature. Higher percentages were measured during the first minutes of a cold start and low ambient temperatures, but the absolute levels were at least two orders of magnitude below the PN limit.

Even though the effectiveness and necessity of GPFs was clearly shown in this paper, more research is necessary for the upcoming Euro 7 regulation, when it is likely that the limit will be lower and the boundary conditions slightly wider. The next generation of GPFs have to be evaluated in particular under a wide range of environmental, driving, and fuel conditions.

Author Contributions: Conceptualization, Z.S. and P.D.; formal analysis, B.G. and V.V.; writing—original draft preparation, B.G.; writing—review and editing, V.V., A.K., A.M., G.M., A.B., J.A., Z.S., P.D. All authors have read and agreed to the published version of the manuscript.

Funding: This research received no external funding.

Data Availability Statement: The data presented in this study are available on request from the corresponding author.

Acknowledgments: The authors would like to acknowledge the technical work of the laboratory personnel L. Bigozzi, C. Bonato, M. Carriero, P. Canevari, M. Centurelli, C. Ferrarese, F. Furni, A. Migneco, M. Otura.

Conflicts of Interest: The authors declare no conflict of interest. The opinions expressed in this manuscript are those of the authors and should in no way be considered to represent an official opinion of the European Commission and the respective institutes. Mention of trade names or commercial products does not constitute endorsement or recommendation by the European Commission, the institutes and/or the authors.

Appendix A

Characteristics of the test cycles.

Table A1. Characteristics of the complete cycles.

	Complete	WLTC	RDE Short	RDE Boundary	RDE Road 1	RDE Road 2
Trip characteristics	Duration (s)	1800	3600	7088	6812	6630
	Distance (km)	23	50	100	96.4	99.0
	Mean speed (km/h)	46.5	49.5	50.9	50.9	53.7
	Max speed (km/h)	131	120	136	149.6	135.2
	95th $v \times a$ (m^2/s^3) ¹	-	-	-	-	-
	Cold start	Yes	Yes	Yes	Yes	Yes
	Temperatures ² (°C)	23 °C	all	−10 °C	20	17
Test mass	Inertia (kg)	1817	1817	2150	1930	1930
Road load coefficients ³	F0 (N)	221	221	253	-	-
	F1 (N/(km/h))	−0.224	−0.224	−0.224	-	-
	F2 (N/(km/h) ²)	0.03147	0.03147	0.03147	-	-
Slope range	(%)	No	−9.6 to 9.2%	−8.1 to 6.5%	−7.3 to 9.2%	−9.8 to 10.6%

¹ Not applicable for complete RDE cycles. ² All refers to −30, −10, 5, 23, and 50 °C. ³ The road-load coefficients (F0–F2) correspond to the road coefficients. The applied dyno coefficients were based on the WLTC coast-down coefficients, modified accordingly for the rest cases. The RDE road mass includes the PEMS, the driver and the co-pilot.

Table A2. Characteristics of the urban cycles (TfL, uphill) and the urban parts of the RDE tests and the WLTC (low and medium phases).

Urban	WLTC	TfL	Uphill Tow	Uphill Tow 85%	RDE Short	RDE Bound.	RDE Road 1	RDE Road 2
Duration (s)	1022	2310	1110	1110	1850	4540	4478	4179
Distance (km)	7.9	8.9	9.2	9.2	12.7	38.0	35.8	34.8
Mean speed (km/h)	27.6	14.0	29.3	29.1	24.7	30.1	28.8	30.0
Max speed (km/h)	76.6	52	53.9	53.0	48.7	60.8	60.0	60
95th $v \times a$ (m^2/s^3) ¹	10.9	7.5	8.7	8.5	10.1 (11.3)	18.7	8.8 (14.8)	9.9 (12.8)
Cold start	Yes	Yes	Yes	Yes	Yes	Yes	Yes	Yes
Temperatures ² (°C)	23 °C	all	−10 °C	−7 °C	all	−10 °C	20	17
Inertia (kg)	1817	1817	2617	3570	1817	2150	1930	1930
F0 (N) ³	221	221	1592	2172	221	253	-	-
F1 (N/(km/h))	−0.224	−0.224	−0.224	−0.224	−0.224	−0.224	-	-
F2 (N/(km/h) ²)	0.03147	0.03147	0.03147	0.03147	0.03147	0.03147	-	-
Slope range (%)	No	No	5% to F0	5% to F0	−9.6 to 8.8%	−8.1 to 6.3%	−7.3 to 9.2%	−9.8 to 10.6%

¹ In brackets following the regulated procedure, i.e., when speeds < 60 km/h from the whole cycle are considered. Outside the brackets for the urban parts defined in Figure 8. The limit is $0.136 v + 14.44$, where v is the mean speed. For example, for 14.1 km/h is $16.3 m^2/s^3$, and for 30.1 km/h it is $18.5 m^2/s^3$. ² All refer to −30, −10, 5, 23, and 50 °C. ³ The road-load coefficients (F0–F2) correspond to the road coefficients. The applied dyno coefficients were based on the WLTC coast-down coefficients, modified accordingly for the rest cases. The RDE road mass includes the PEMS, the driver and the co-pilot.

Table A3. Characteristics of the motorway cycle (BAB), the extra-high part of WLTC and the motorway parts of the RDE cycles.

Motorway	WLTC	BAB	RDE Short	RDE Boundary	RDE Road 1	RDE Road 2
Duration (s)	323	800	700	1091	881	1054
Distance (km)	8.3	25	19.1	32.2	29.0	34.2
Mean speed (km/h)	94.0	112.7	98.5	106.3	118.4	116.8
Max speed (km/h)	131.3	130	121	138	148.8	135.2
95th $v \times a$ (m^2/s^3) ¹	15.1	43.5	13.7	26.7	24.9 (23.0)	21.5 (17.9)
Cold start	No	No	No	No	No	No
Temperatures ² (°C)	23 °C	all	all	−10 °C	20	17
Inertia (kg)	1817	1817	1817	2150	1930	1930
F0 (N) ³	221	221	221	253	-	-
F1 (N/(km/h))	−0.224	−0.224	−0.224	−0.224	-	-
F2 (N/(km/h) ²)	0.03147	0.03147	0.03147	0.03147	-	-
Slope range (%)	No	No	−5.1 to 6.4%	−5.0 to 5.3%	−6.6 to 6.2%	−7.2 to 5.8%

¹ In brackets following the regulated procedure, i.e., when speeds >90 km/h from the whole cycle are considered. Outside the brackets for the urban parts defined in Figure 8. The limit is $0.0742 v + 18.966$, where v is the mean speed. For example, for 94 km/h it is $25.9 m^2/s^3$, and for 118.4 km/h it is $27.8 m^2/s^3$. ² All refer to −30, −10, 5, 23, and 50 °C. ³ The road-load coefficients (F0–F2) correspond to the road coefficients. The applied dyno coefficients were based on the WLTC coast-down coefficients, modified accordingly for the rest cases. The RDE road mass includes the PEMS, the driver and the co-pilot.

Figure A1 plots coolant temperatures as registered from the OBD (on-board diagnostics). Note that the recordings from the 23 °C day were not available. The morning TfL tests after >12 h soaking had an almost identical starting temperature with the evening RDE short tests after 6 h of forced cooling.

Figure A2 plots exhaust gas temperatures for the complete cycles (TfL + BAB) and RDE short. The start temperature is higher than the ambient temperature due to the heat transfer from the heated lines of the analyzers connected to the tailpipe.

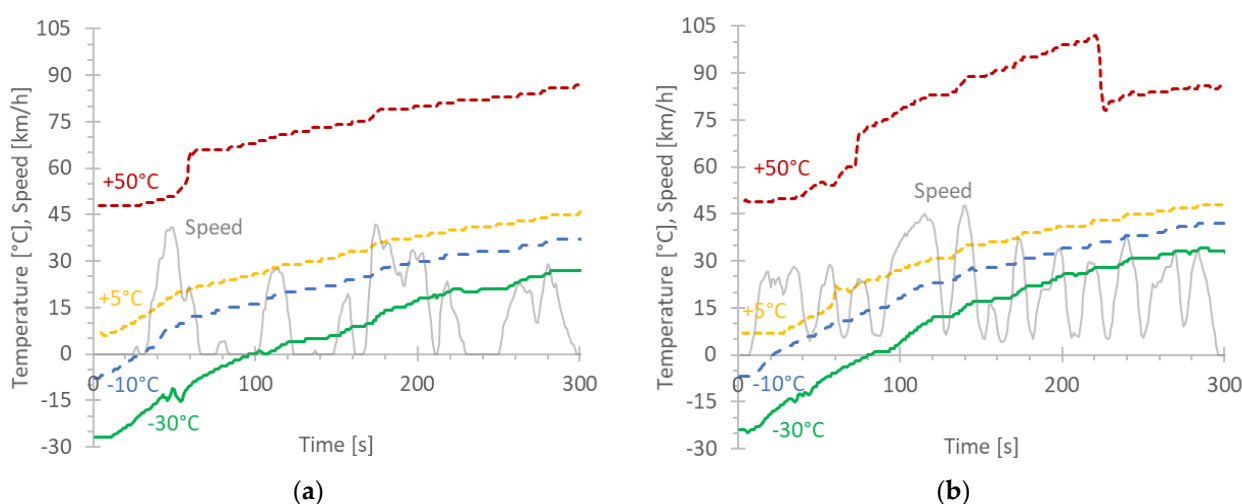


Figure A1. Coolant temperature during cold start (300 s): (a) TfL; (b) RDE short.

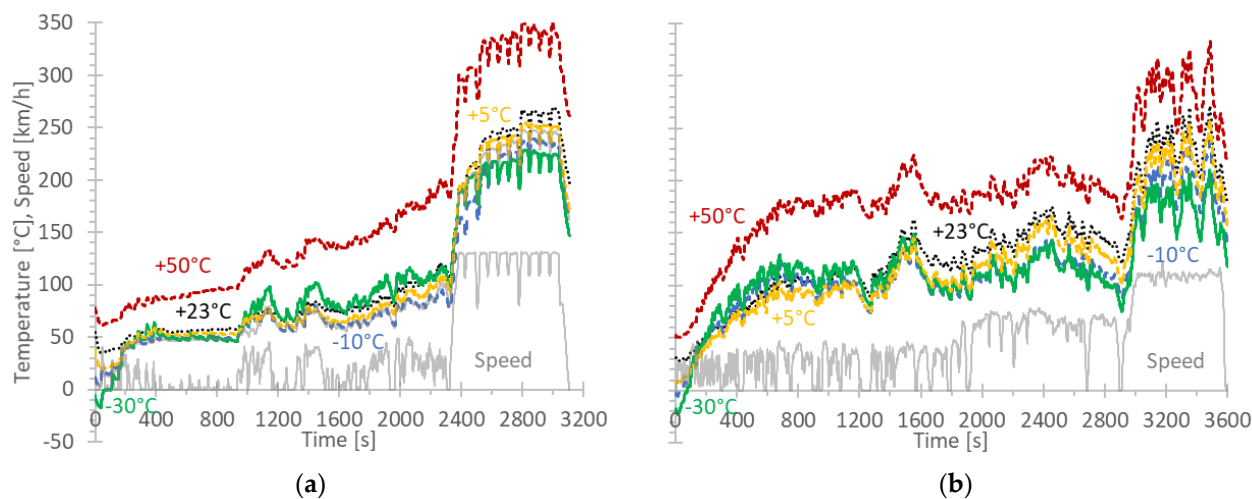


Figure A2. Exhaust gas temperature: (a) TfL + BAB; (b) RDE short.

References

1. European Environment Agency. *Air Quality in Europe: 2020 Report*; Publications Office of the European Union: Luxembourg, 2020. [[CrossRef](#)]
2. Health Effects Institute. *State of Global Air 2020*; Health Effects Institute: Boston, MA, USA, 2020.
3. Liu, C.; Chen, R.; Sera, F.; Vicedo-Cabrera, A.M.; Guo, Y.; Tong, S.; Coelho, M.S.Z.S.; Saldiva, P.H.N.; Lavigne, E.; Matus, P.; et al. Ambient Particulate Air Pollution and Daily Mortality in 652 Cities. *N. Engl. J. Med.* **2019**, *381*, 705–715. [[CrossRef](#)]
4. Wyzga, R.E.; Rohr, A.C. Long-Term Particulate Matter Exposure: Attributing Health Effects to Individual PM Components. *J. Air Waste Manag. Assoc.* **2015**, *65*, 523–543. [[CrossRef](#)]
5. Yang, Y.; Pun, V.C.; Sun, S.; Lin, H.; Mason, T.G.; Qiu, H. Particulate Matter Components and Health: A Literature Review on Exposure Assessment. *J. Public Health Emerg.* **2018**, *2*, 14. [[CrossRef](#)]

6. Li, N.; Georas, S.; Alexis, N.; Fritz, P.; Xia, T.; Williams, M.A.; Horner, E.; Nel, A. A Work Group Report on Ultrafine Particles (American Academy of Allergy, Asthma & Immunology): Why Ambient Ultrafine and Engineered Nanoparticles Should Receive Special Attention for Possible Adverse Health Outcomes in Human Subjects. *J. Allergy Clin. Immunol.* **2016**, *138*, 386–396. [[CrossRef](#)] [[PubMed](#)]
7. Kwon, H.-S.; Ryu, M.H.; Carlsten, C. Ultrafine Particles: Unique Physicochemical Properties Relevant to Health and Disease. *Exp. Mol. Med.* **2020**, *52*, 318–328. [[CrossRef](#)]
8. IBGE (Institut Bruxellois Pour La Gestion De L'Environnement). *Plan. Regional Air-Climat-Energie*; Bruxelles Environnement/Département Planification Air, Climat et Energie: Brussels, Belgium, 2016. Available online: https://document.environnement.brussels/opac_css/elecfile/PLAN_AIR_CLIMAT_ENERGIE_FR_DEF.pdf (accessed on 10 May 2021).
9. Donzelli, G.; Cioni, L.; Cancellieri, M.; Llopis Morales, A.; Morales Suárez-Varela, M. The Effect of the Covid-19 Lockdown on Air Quality in Three Italian Medium-Sized Cities. *Atmosphere* **2020**, *11*, 1118. [[CrossRef](#)]
10. Fu, F.; Purvis-Roberts, K.L.; Williams, B. Impact of the Covid-19 Pandemic Lockdown on Air Pollution in 20 Major Cities around the World. *Atmosphere* **2020**, *11*, 1189. [[CrossRef](#)]
11. Grivas, G.; Athanasopoulou, E.; Kakouri, A.; Bailey, J.; Liakakou, E.; Stavroulas, I.; Kalkavouras, P.; Bougiatioti, A.; Kaskaoutis, D.; Ramonet, M.; et al. Integrating in Situ Measurements and City Scale Modelling to Assess the Covid-19 Lockdown Effects on Emissions and Air Quality in Athens, Greece. *Atmosphere* **2020**, *11*, 1174. [[CrossRef](#)]
12. Menut, L.; Bessagnet, B.; Siour, G.; Mailler, S.; Pennel, R.; Cholakian, A. Impact of Lockdown Measures to Combat Covid-19 on Air Quality over Western Europe. *Sci. Total Environ.* **2020**, *741*, 140426. [[CrossRef](#)] [[PubMed](#)]
13. Kumari, P.; Toshniwal, D. Impact of Lockdown on Air Quality over Major Cities across the Globe during Covid-19 Pandemic. *Urban. Clim.* **2020**, *34*, 100719. [[CrossRef](#)]
14. de Jesus, A.L.; Rahman, M.M.; Mazaheri, M.; Thompson, H.; Knibbs, L.D.; Jeong, C.; Evans, G.; Nei, W.; Ding, A.; Qiao, L.; et al. Ultrafine Particles and PM_{2.5} in the Air of Cities around the World: Are They Representative of Each Other? *Environ. Int.* **2019**, *129*, 118–135. [[CrossRef](#)]
15. Mock, P. *European Vehicle Market. Statistics: Pocketbook 2020/21*; International Council on Clean Transportation Europe: Berlin, Germany, 2020.
16. Giechaskiel, B.; Joshi, A.; Ntziachristos, L.; Dilara, P. European Regulatory Framework and Particulate Matter Emissions of Gasoline Light-Duty Vehicles: A Review. *Catalysts* **2019**, *9*, 586. [[CrossRef](#)]
17. Chan, T.W.; Meloche, E.; Kubsh, J.; Rosenblatt, D.; Brezny, R.; Rideout, G. Evaluation of a Gasoline Particulate Filter to Reduce Particle Emissions from a Gasoline Direct Injection Vehicle. *SAE Int. J. Fuels Lubr.* **2012**, *5*, 1277–1290. [[CrossRef](#)]
18. Jang, J.; Lee, J.; Choi, Y.; Park, S. Reduction of Particle Emissions from Gasoline Vehicles with Direct Fuel Injection Systems Using a Gasoline Particulate Filter. *Sci. Total Environ.* **2018**, *644*, 1418–1428. [[CrossRef](#)]
19. Suarez-Bertoa, R.; Lähde, T.; Pavlovic, J.; Valverde, V.; Clairotte, M.; Giechaskiel, B. Laboratory and On-Road Evaluation of a GPF-Equipped Gasoline Vehicle. *Catalysts* **2019**, *9*, 678. [[CrossRef](#)]
20. Giechaskiel, B.; Woodburn, J.; Szczołka, A.; Bielaczyc, P. *Particulate Matter (PM) Emissions of Euro 5 and Euro 6 Vehicles Using Systems with Evaporation Tube or Catalytic Stripper and 23 nm or 10 nm Counters*; SAE Technical Paper 2020-01-2203; SAE: Warrendale, PA, USA, 2020. [[CrossRef](#)]
21. Samaras, Z.C.; Andersson, J.; Bergmann, A.; Hausberger, S.; Toumasatos, Z.; Keskinen, J.; Haisch, C.; Kontses, A.; Ntziachristos, L.D.; Landl, L.; et al. *Measuring Automotive Exhaust Particles Down to 10 nm*; SAE Technical Paper 2020-01-2209; SAE: Warrendale, PA, USA, 2020. [[CrossRef](#)]
22. Hu, Z.; Lu, Z.; Song, B.; Quan, Y. Impact of Test Cycle on Mass, Number and Particle Size Distribution of Particulates Emitted from Gasoline Direct Injection Vehicles. *Sci. Total Environ.* **2021**, *762*, 143128. [[CrossRef](#)] [[PubMed](#)]
23. Zhang, R.; Howard, K.; Kirkman, P.; Browne, D.; Lu, Z.; He, S.; Boger, T. *A Study into the Impact of Engine Oil on Gasoline Particulate Filter Performance through a Real-World Fleet Test*; SAE Technical Paper 2019-01-0299; SAE: Warrendale, PA, USA, 2019. [[CrossRef](#)]
24. Sterlepper, S.; Claßen, J.; Pischinger, S.; Schernus, C.; Görden, M.; Cox, J.; Nijs, M.; Scharf, J.; Rose, D.; Boger, T. *Analysis of the Emission Conversion Performance of Gasoline Particulate Filters over Lifetime*; SAE Technical Paper 2019-24-0156; SAE: Warrendale, PA, USA, 2019. [[CrossRef](#)]
25. Mamakos, A.; Martini, G.; Manfredi, U. Assessment of the Legislated Particle Number Measurement Procedure for a Euro 5 and a Euro 6 Compliant Diesel Passenger Cars under Regulated and Unregulated Conditions. *J. Aerosol Sci.* **2013**, *55*, 31–47. [[CrossRef](#)]
26. Demuyneck, J.; Favre, C.; Bosteels, D.; Hamje, H.; Andersson, J. *Real-World Emissions Measurements of a Gasoline Direct Injection Vehicle without and with a Gasoline Particulate Filter*; SAE Technical Paper 2017-01-0985; SAE: Warrendale, PA, USA, 2017. [[CrossRef](#)]
27. Chan, T.W.; Meloche, E.; Kubsh, J.; Brezny, R. Black Carbon Emissions in Gasoline Exhaust and a Reduction Alternative with a Gasoline Particulate Filter. *Environ. Sci. Technol.* **2014**, *48*, 6027–6034. [[CrossRef](#)] [[PubMed](#)]
28. Giechaskiel, B.; Bonnel, P.; Perujo, A.; Dilara, P. Solid Particle Number (SPN) Portable Emissions Measurement Systems (PEMS) in the European Legislation: A Review. *Int. J. Environ. Res. Public Health* **2019**, *16*, 4819. [[CrossRef](#)] [[PubMed](#)]
29. Dorscheidt, F.; Sterlepper, S.; Görden, M.; Nijs, M.; Claßen, J.; Yadla, S.K.; Maurer, R.; Pischinger, S.; Krysmo, S.; Abdelkader, A. *Gasoline Particulate Filter Characterization Focusing on the Filtration Efficiency of Nano-Particulates Down to 10 nm*; SAE Technical Paper 2020-01-2212; SAE: Warrendale, PA, USA, 2020. [[CrossRef](#)]

30. Bannister, C.D.; Taylor, J. Analysis and Empirical Modelling to Assess and Predict the Impact of Catalyst Light-off Strategies on the Exhaust Gas Temperatures of Spark Ignition Engines. *Proc. Inst. Mech. Eng. Part D J. Automob. Eng.* **2014**, *228*, 1644–1653. [[CrossRef](#)]
31. Gao, J.; Tian, G.; Sornioti, A.; Karci, A.E.; Di Palo, R. Review of Thermal Management of Catalytic Converters to Decrease Engine Emissions during Cold Start and Warm Up. *Appl. Therm. Eng.* **2019**, *147*, 177–187. [[CrossRef](#)]
32. Di Iorio, S.; Catapano, F.; Sementa, P.; Vaglieco, B.M.; Nicol, G.; Sgroi, M.F. *Sub-23 nm Particle Emissions from Gasoline Direct Injection Vehicles and Engines: Sampling and Measure*; SAE Technical Paper 2020-01-0396; SAE: Warrendale, PA, USA, 2020. [[CrossRef](#)]
33. Filippo, A.D.; Maricq, M.M. Diesel Nucleation Mode Particles: Semivolatile or Solid? *Environ. Sci. Technol.* **2008**, *42*, 7957–7962. [[CrossRef](#)]
34. Giechaskiel, B.; Manfredi, U.; Martini, G. Engine Exhaust Solid Sub-23 Nm Particles: I. Literature Survey. *SAE Int. J. Fuels Lubr.* **2014**, *7*, 950–964. [[CrossRef](#)]
35. An, Y.; Teng, S.; Pei, Y.; Qin, J.; Li, X.; Zhao, H. An Experimental Study of Polycyclic Aromatic Hydrocarbons and Soot Emissions from a GDI Engine Fueled with Commercial Gasoline. *Fuel* **2016**, *164*, 160–171. [[CrossRef](#)]
36. Yang, J.; Roth, P.; Durbin, T.D.; Johnson, K.C.; Cocker, D.R.; Asa-Awuku, A.; Brezny, R.; Geller, M.; Karavalakis, G. Gasoline Particulate Filters as an Effective Tool to Reduce Particulate and Polycyclic Aromatic Hydrocarbon Emissions from Gasoline Direct Injection (GDI) Vehicles: A Case Study with Two GDI Vehicles. *Environ. Sci. Technol.* **2018**, *52*, 3275–3284. [[CrossRef](#)]
37. Chen, L.; Liang, Z.; Zhang, X.; Shuai, S. Characterizing Particulate Matter Emissions from GDI and PFI Vehicles under Transient and Cold Start Conditions. *Fuel* **2017**, *189*, 131–140. [[CrossRef](#)]
38. Zhu, R.; Hu, J.; Bao, X.; He, L.; Lai, Y.; Zu, L.; Li, Y.; Su, S. Tailpipe Emissions from Gasoline Direct Injection (GDI) and Port Fuel Injection (PFI) Vehicles at Both Low and High Ambient Temperatures. *Environ. Pollut.* **2016**, *216*, 223–234. [[CrossRef](#)]
39. Giechaskiel, B.; Mamakos, A.; Andersson, J.; Dilara, P.; Martini, G.; Schindler, W.; Bergmann, A. Measurement of Automotive Nonvolatile Particle Number Emissions within the European Legislative Framework: A Review. *Aerosol Sci. Technol.* **2012**, *46*, 719–749. [[CrossRef](#)]
40. Chan, T.W.; Saffaripour, M.; Liu, F.; Hendren, J.; Thomson, K.A.; Kubsh, J.; Brezny, R.; Rideout, G. Characterization of Real-Time Particle Emissions from a Gasoline Direct Injection Vehicle Equipped with a Catalyzed Gasoline Particulate Filter during Filter Regeneration. *Emiss. Control Sci. Technol.* **2016**, *2*, 75–88. [[CrossRef](#)]
41. Myung, C.-L.; Kim, J.; Jang, W.; Jin, D.; Park, S.; Lee, J. Nanoparticle Filtration Characteristics of Advanced Metal Foam Media for a Spark Ignition Direct Injection Engine in Steady Engine Operating Conditions and Vehicle Test Modes. *Energies* **2015**, *8*, 1865–1881. [[CrossRef](#)]
42. Suarez-Bertoa, R.; Astorga, C. Impact of Cold Temperature on Euro 6 Passenger Car Emissions. *Environ. Pollut.* **2018**, *234*, 318–329. [[CrossRef](#)]
43. Weber, C.; Sundvor, I.; Figenbaum, E. Comparison of Regulated Emission Factors of Euro 6 LDV in Nordic Temperatures and Cold Start Conditions: Diesel- and Gasoline Direct-Injection. *Atmos. Environ.* **2019**, *206*, 208–217. [[CrossRef](#)]
44. Bielaczyc, P.; Woodburn, J.; Szczotka, A. *Investigations into Particulate Emissions from Euro 5 Passenger Cars with DISI Engines Tested at Multiple Ambient Temperatures*; SAE Technical Paper 2015-24-2517; SAE: Warrendale, PA, USA, 2015. [[CrossRef](#)]
45. He, L.; Hu, J.; Zhang, S.; Wu, Y.; Zhu, R.; Zu, L.; Bao, X.; Lai, Y.; Su, S. The Impact from the Direct Injection and Multi-Port Fuel Injection Technologies for Gasoline Vehicles on Solid Particle Number and Black Carbon Emissions. *Appl. Energy* **2018**, *226*, 819–826. [[CrossRef](#)]
46. Ristimäki, J.; Keskinen, J.; Virtanen, A.; Maricq, M.; Aakko, P. Cold Temperature PM Emissions Measurement: Method Evaluation and Application to Light Duty Vehicles. *Environ. Sci. Technol.* **2005**, *39*, 9424–9430. [[CrossRef](#)]
47. Brandenberger, S.; Mohr, M.; Grob, K.; Neukom, H.P. Contribution of Unburned Lubricating Oil and Diesel Fuel to Particulate Emission from Passenger Cars. *Atmos. Environ.* **2005**, *39*, 6985–6994. [[CrossRef](#)]
48. Zhang, L.; He, S.; Zhang, Q.; Liao, Y.; Zhang, H. *Gasoline Particulate Filter Applications for Plug-in Hybrid and Traditional Cars*; SAE Technical Paper 2020-01-1430; SAE: Warrendale, PA, USA, 2020. [[CrossRef](#)]
49. Momenimovahed, A.; Handford, D.; Checkel, M.D.; Olfert, J.S. Particle Number Emission Factors and Volatile Fraction of Particles Emitted from On-Road Gasoline Direct Injection Passenger Vehicles. *Atmos. Environ.* **2015**, *102*, 105–111. [[CrossRef](#)]
50. Chan, T.W.; Lax, D.; Gunter, G.C.; Hendren, J.; Kubsh, J.; Brezny, R. Assessment of the Fuel Composition Impact on Black Carbon Mass, Particle Number Size Distributions, Solid Particle Number, Organic Materials, and Regulated Gaseous Emissions from a Light-Duty Gasoline Direct Injection Truck and Passenger Car. *Energy Fuels* **2017**, *31*, 10452–10466. [[CrossRef](#)]
51. Choi, K.; Kim, J.; Ko, A.; Myung, C.-L.; Park, S.; Lee, J. Size-Resolved Engine Exhaust Aerosol Characteristics in a Metal Foam Particulate Filter for GDI Light-Duty Vehicle. *J. Aerosol Sci.* **2013**, *57*, 1–13. [[CrossRef](#)]
52. Yamada, H.; Inomata, S.; Tanimoto, H. Particle and VOC Emissions from Stoichiometric Gasoline Direct Injection Vehicles and Correlation between Particle Number and Mass Emissions. *Emiss. Control Sci. Technol.* **2017**, *3*, 135–141. [[CrossRef](#)]
53. Kim, K.; Chung, W.; Kim, M.; Kim, C.; Myung, C.-L.; Park, S. Inspection of PN, CO₂, and Regulated Gaseous Emissions Characteristics from a GDI Vehicle under Various Real-World Vehicle Test Modes. *Energies* **2020**, *13*, 2581. [[CrossRef](#)]
54. Dimopoulos Eggenschwiler, P.; Schreiber, D.; Schröter, K. Characterization of the Emission of Particles Larger than 10 Nm in the Exhaust of Modern Gasoline and CNG Light Duty Vehicles. *Fuel* **2021**, *291*, 120074. [[CrossRef](#)]

55. Lenz, M.; Cremer, M.; Guse, D.; Röhrich, H.; Pischinger, S. A Case Study on Particulate Emissions from a Gasoline Plug-in Hybrid Electric Vehicle during Engine Warm-up, Taking into Account Start-Stop Operation. *Proc. Inst. Mech. Eng. Part D J. Automob. Eng.* **2020**, *234*, 2907–2922. [[CrossRef](#)]
56. Sun, Y.; Dong, W.; Yu, X. Effects of Coolant Temperature Coupled with Controlling Strategies on Particulate Number Emissions in GDI Engine under Idle Stage. *Fuel* **2018**, *225*, 1–9. [[CrossRef](#)]
57. Karjalainen, P.; Pirjola, L.; Heikkilä, J.; Lähde, T.; Tzamkiozis, T.; Ntziachristos, L.; Keskinen, J.; Rönkkö, T. Exhaust Particles of Modern Gasoline Vehicles: A Laboratory and an on-Road Study. *Atmos. Environ.* **2014**, *97*, 262–270. [[CrossRef](#)]
58. Tabata, K.; Takahashi, M.; Takeda, K.; Tsurumi, K.; Kiya, Y.; Tobe, S.; Ogura, A. *Studies on Characteristics of Nanoparticles Generated in a Gasoline Direct-Injection Engine*; SAE Technical Paper 2019-01-2328; SAE: Warrendale, PA, USA, 2019. [[CrossRef](#)]
59. Tang, W.; Siani, A.; Chen, F.; Chen, B. *On Developing Advanced Catalysts Systems to Meet China New Regulations*; SAE Technical Paper 2019-01-0978; SAE: Warrendale, PA, USA, 2019. [[CrossRef](#)]
60. Adam, F.; Olfert, J.; Wong, K.-F.; Kunert, S.; Richter, J.M. *Effect of Engine-Out Soot Emissions and the Frequency of Regeneration on Gasoline Particulate Filter Efficiency*; SAE Technical Paper 2020-01-1431; SAE: Warrendale, PA, USA, 2020. [[CrossRef](#)]
61. Wang, Y.; Wang, J.; Hao, C.; Wang, X.; Li, Q.; Zhai, J.; Ge, Y.; Hao, L.; Tan, J. Characteristics of Instantaneous Particle Number (PN) Emissions from Hybrid Electric Vehicles under the Real-World Driving Conditions. *Fuel* **2021**, *286*, 119466. [[CrossRef](#)]
62. Saffaripour, M.; Chan, T.W.; Liu, F.; Thomson, K.A.; Smallwood, G.J.; Kubsh, J.; Brezny, R. Effect of Drive Cycle and Gasoline Particulate Filter on the Size and Morphology of Soot Particles Emitted from a Gasoline-Direct-Injection Vehicle. *Environ. Sci. Technol.* **2015**, *49*, 11950–11958. [[CrossRef](#)]
63. Maricq, M.M.; Szente, J.J.; Harwell, A.L.; Loos, M.J. Impact of Aggressive Drive Cycles on Motor Vehicle Exhaust PM Emissions. *J. Aerosol Sci.* **2017**, *113*, 1–11. [[CrossRef](#)]
64. Giechaskiel, B. Particle Number Emissions of a Diesel Vehicle during and between Regeneration Events. *Catalysts* **2020**, *10*, 587. [[CrossRef](#)]
65. Claßen, J.; Pischinger, S.; Krysmo, S.; Sterlepper, S.; Dorscheidt, F.; Doucet, M.; Reuber, C.; Görgen, M.; Scharf, J.; Nijs, M.; et al. Statistically Supported Real Driving Emission Calibration: Using Cycle Generation to Provide Vehicle-Specific and Statistically Representative Test Scenarios for Euro 7. *Int. J. Engine Res.* **2020**, *21*, 1783–1799. [[CrossRef](#)]
66. Kurtyka, K.; Pielecha, J. The Evaluation of Exhaust Emission in RDE Tests Including Dynamic Driving Conditions. *Transp. Res. Procedia* **2019**, *40*, 338–345. [[CrossRef](#)]
67. Boger, T.; Glasson, T.; Rose, D.; Ingram-Ogunwumi, R.; Wu, H. *Next Generation Gasoline Particulate Filters for Uncatalyzed Applications and Lowest Particulate Emissions*; SAE Technical Paper 2021-01-0584; SAE: Warrendale, PA, USA, 2021. [[CrossRef](#)]
68. Pan, J.; Hua, L.; Lin, Y.; Liu, S.; Zhang, J.; Zhao, L.; Richter, J.M.; Kunert, S.; Schoenhauer, J.; Gieshoff, J. *Experimental Study on the Impact of Lubricant Ash on CN6 After-Treatment System Performance of GDI Vehicle*; SAE Technical Paper 2021-01-0586; SAE: Warrendale, PA, USA, 2021. [[CrossRef](#)]
69. Zhao, Y.; Li, X.; Hu, S.; Ma, C. Effects of the Particulate Matter Index and Particulate Evaluation Index of the Primary Reference Fuel on Particulate Emissions from Gasoline Direct Injection Vehicles. *Atmosphere* **2019**, *10*, 111. [[CrossRef](#)]
70. Raza, M.; Chen, L.; Leach, F.; Ding, S. A Review of Particulate Number (PN) Emissions from Gasoline Direct Injection (GDI) Engines and Their Control Techniques. *Energies* **2018**, *11*, 1417. [[CrossRef](#)]
71. Zinola, S.; Leblanc, M.; Rouleau, L.; Dunand, X.; Baltzopoulou, P.; Chasapidis, L.; Deloglou, D.; Melas, A.D.; Konstandopoulos, A.G.; Rüggeberg, T.; et al. *Measurement of Sub-23 nm Particles Emitted by Gasoline Direct Injection Engine with New Advanced Instrumentation*; SAE Technical Paper 2019-01-2195; SAE: Warrendale, PA, USA, 2019. [[CrossRef](#)]
72. Singh, R.; Voice, A.; Fatouraie, M.; Levy, R. *Fuel Effects on Engine-out Emissions Part 1—Comparing Certification and Market Gasoline Fuels*; SAE Technical Paper 2021-01-0541; SAE: Warrendale, PA, USA, 2021. [[CrossRef](#)]
73. Joshi, A. *Review of Vehicle Engine Efficiency and Emissions*; SAE Technical Paper 2021-01-0575; SAE: Warrendale, PA, USA, 2021. [[CrossRef](#)]
74. Giechaskiel, B.; Cresnoverh, M.; Jörgl, H.; Bergmann, A. Calibration and Accuracy of a Particle Number Measurement System. *Meas. Sci. Technol.* **2010**, *21*, 045102. [[CrossRef](#)]
75. Samaras, Z.; Andersson, J.; Aakko-Saksa, P.; Cuelenaere, R.; Mellios, G. Additional Technical Issues for Euro 7 (LDV) 2021. In Proceedings of the AGVES Meeting, Webex, 27 April 2021.